Materials Science and Engineering C 62 (2016) 260–267

Contents lists available at ScienceDirect

Materials Science and Engineering C

journal homepage: www.elsevier.com/locate/msec

The comparison study of bioactivity between composites containing synthetic non-substituted and carbonate-substituted hydroxyapatite

Leszek Borkowski [a,*], Anna Sroka-Bartnicka [b], Piotr Drączkowski [c], Agnieszka Ptak [a], Emil Zięba [d], Anna Ślósarczyk [e], Grażyna Ginalska [a]

[a] Chair and Department of Biochemistry and Biotechnology, Medical University of Lublin, Chodźki 1, 20-093 Lublin, Poland
[b] Department of Biopharmacy, Medical University of Lublin, Chodźki 4a, 20-093 Lublin, Poland
[c] Department of Synthesis and Chemical Technology of Pharmaceutical Substances, Medical University of Lublin, Chodźki 4a, 20-093 Lublin, Poland
[d] SEM Laboratory, Department of Zoology and Ecology, John Paul II Catholic University of Lublin, Al. Kraśnicka 102, 20-718 Lublin, Poland
[e] Faculty of Materials Science and Ceramics, AGH-University of Science and Technology, Mickiewicza 30, 30-059 Krakow, Poland

ARTICLE INFO

Article history:
Received 28 July 2015
Received in revised form 12 January 2016
Accepted 23 January 2016
Available online 26 January 2016

Keywords:
Apatite
Bioactivity
Bone
Composite
Raman spectroscopy

ABSTRACT

Apatite forming ability of hydroxyapatite (HAP) and carbonate hydroxyapatite (CHAP) containing composites was compared. Two composite materials, intended for filling bone defects, were made of polysaccharide polymer and one of two types of hydroxyapatite. The bioactivity of the composites was evaluated *in vitro* by soaking in a simulated body fluid (SBF), and the formation of the apatite layer was determined by scanning electron microscopy with energy-dispersive spectrometer and Raman spectroscopy. The results showed that both the composites induced the formation of apatite layer on their surface after soaking in SBF. In addition, the sample weight changes and the ion concentration of the SBF were scrutinized. The results showed the weight increase for both materials after SBF treatment, higher weight gain and higher uptake of calcium ions by HAP containing scaffolds. SBF solution analysis indicated loss of calcium and phosphorus ions during experiment. All these results indicate apatite forming ability of both biomaterials and suggest comparable bioactive properties of composite containing pure hydroxyapatite and carbonate-substituted one.

1. Introduction

Hydroxyapatite (HAP) is the most frequently used representative of calcium phosphates in commercially available ceramic-based bone substitute materials. It has been widely used in medicine and dentistry for more than 40 years, because of its good biocompatibility with hard human tissues and osteoconductive properties [1]. Mostly it is used as pure, non-substituted HAP in the form of ceramic (such products as: Osteograf/D®, Osteogen®, Osprovit®, Endobon®, OSTIM®), ceramic composites (eg. 4BONE®, Camceram®, BoneSave®, ProOsteon®, HT Biocer®, NanoBone®) or ceramic-polymer composites (Healos®). However, biological apatite present in bone is a carbonate-substituted one of a low crystallinity. Carbonate ions (present in bone and dentine tissues at the level of 2.3–8 wt.% [2] were claimed to increase the solubility and decrease the crystallinity of ceramics [3,4]. Therefore, there is growing interest in the potential application of carbonate-substituted hydroxyapatite (CHAP, also called as *biomimetic*) in bone tissue engineering. Up to now, CHAP found an application as a coating on metals, mostly titanium [5,6,7,8,9] and polymers [10,11,12]. Numerous studies were performed on CHAP containing scaffolds either in the form of ceramic [13,14,15,16,17,18] or ceramic-based composites [19,20,21,22]. The results of *in vitro* studies on ceramics showed the enhanced attachment and proliferation of rat osteoblasts as well as the formation of mineralization nodules in comparison with non-substituted HAP. On the other hand, some investigators report that carbonate substitution can either delay or accelerate the proliferation of osteoblastic-like cells and constrain the osteoclastic differentiation. The studies on CHAP-based composites lead to the general conclusion that addition of CHAP affects the bioactivity of the composites, increases adhesion and differentiation of osteoblast cells, collagen and osteocalcin expression and mineral deposition. Similarly, *in vivo* studies do not provide explicit conclusions concerning the biological impact of carbonate-substituted hydroxyapatite [23,24,25,26,27]. On the basis of literature analysis, it seems that there is still a high need to explore the difference in properties between HAP and CHAP.

Bioactivity of biomaterials is described as its ability to bond with host bone tissue [1]. The mechanism of bone bonding is through the formation of a surface layer of apatite, which is similar to the mineral component of bone. Currently, two common methods have been used for testing the *in vitro* bioactivity of biomedical materials. One method (also called the biomineralization test) is to evaluate the apatite-formation ability of biomaterials in the simulated body fluids (SBFs) [28]. It was firstly established by Kokubo and colleagues in 1990 to

* Corresponding author.
E-mail address: leszek.borkowski@umlub.pl (L. Borkowski).

http://dx.doi.org/10.1016/j.msec.2016.01.056
0928-4931/

assess bioactive potential of ceramics [29,30]. The second method is to investigate the effect of material on osteogenic differentiation using cell experiments [13,31,32,33]. Selection of methods for the evaluation of *in vitro* bioactivity of biomaterials depends on the composition of materials and the mechanism of their bone formation [34].

In this study we compared apatite forming ability of hydroxyapatite and carbonate hydroxyapatite using two recently developed ceramic-polymer composite materials [35,36]. Two types of scaffolds contained HAP or CHAP granules and the same polysaccharide (β-1,3-glucan) playing a role of joining and elasticity increasing agent. The polymer used in these composites is a natural, relatively cheap, non-animal and nontoxic glucan. It has already been commercialized as a formulation aid, processing aid, stabilizer and thickener or texturizer in foods [37]. The bioactive properties of HAP and CHAP were assessed by detailed examination of precipitated hydroxycarbonate layer on the surface of polymer. The investigation was conducted in SBF under semi-dynamic conditions for 1 month. *In vitro* composite mineralization was analysed qualitatively and quantitatively, using such tools as scanning electron microscopy (SEM), an energy dispersive X-ray detector (EDS) and Raman mapping.

2. Materials and methods

2.1. Composite preparation

12 CHAP-glucan composite and 12 HAP-glucan composite scaffolds were prepared according to the procedure described in european patent [38]. Briefly, samples were fabricated by mixing 3 g of CHAP or HAP granules with β-1,3-glucan aqueous suspension (0.625 g of glucan + 5 ml of distilled water), thus obtaining wt.% proportion granules to β-1,3-glucan 83:17. The mixture of ceramic/glucan solution was put into a special glass mould and baked at 90 °C for 15 min. Finally, the fabricated material was cut with scalpel into cubes with the side length of 10 mm (±1), dried for 4 days at 37 °C, subjected to exsiccation for the next 3 days and sterilized.

CHAP and HAP granules were synthesized at the AGH-University of Science, according to patented procedures [39,40]. Physicochemical data of the HAP/CHAP granules and the HAP/glucan and CHAP/glucan composite samples were presented in Tables 1 and 2.

β-1,3-Glucan (curdlan) from *Alcaligenes faecalis* (DP 450) was supplied by Wako Chemicals, Japan.

2.2. Soaking in a semi-dynamic SBF conditions

Prior to the experiment, all composite samples were weigh on an analytical balance with accuracy 0.0000 g. Laboratory glassware was washed, soaked for 24 h in HCl, rinsed with distilled water and autoclaved. The SBF was prepared by dissolving reagent grade NaCl, $NaHCO_3$, KCl, K_2HPO_4, $MgCl_2 \cdot 6H_2O$, $CaCl_2$ and Na_2SO_4 into ultra-pure water, $(CH_2OH)_3CNH_3$ was added and the solution was buffered at pH 7.25 with HCl (according to the method proposed by Kokubo et al., [29]). Afterwards, the fluid was sterilized by mechanical filtration, using the Stericup filter (500 ml, 0.22 μm; Millipore Corporation) under vacuum.

During experiment the composite samples were named as follows:

- CHAP Composite — treated in SBF (n = 9)
- HAP Composite — treated in SBF (n = 9)
- CHAP Control — treated in water (n = 3)
- HAP Control — treated in water (n = 3)

CHAP and HAP Composite samples were soaked in 100-ml bottles (Simax, Czech Republic) with 80 ml of SBF (one bottle contained 3 samples). The SBF solution was replaced with new every 2–3 days to ensure sufficient ion concentrations for mineral growth. Control samples were kept in 80 ml of ultra-pure water. Incubation was conducted at 37 °C for various periods: 10, 20 and 30 days. After a given period, the specimens were dried for 4 days at 37 °C, subjected to exsiccation for the next 3 days and weighed.

Quantitative analysis (weight measurements) was performed for samples treated with SBF for 10, 20 and 30 days. Structural analysis of the scaffolds (aimed at showing the presence of apatite crystals on the surface of composites) was performed on the samples after 30-day SBF-treatment because the differences between CHAP and HAP Composites were the highest.

2.3. Structural analysis of the samples

2.3.1. SEM–EDS

The polymeric surface of specimens before and after soaking in SBF wasanalysed using scanning electron microscopy (FE-SEM; Zeiss ULTRA plus) with an energy dispersive X-ray detector (EDS; Bruker). The regions of interest (polymer phase of composites) for EDS analysis were defined using magnified SEM micrographs. The chemical composition (presented in wt.%) was calculated automatically by software on the basis of EDS spectra.

2.3.2. Raman spectroscopy and mapping

2.3.2.1. Spatial distribution. The Raman experiments were performed using a DXR confocal Raman Microscope equipped with the Omnic™ 8 software from Thermo Fisher Scientific (Madison, WI, USA) and a X–Y motorized sample stage. The excitation laser wavelength was 780 nm. Filters of 780 nm and 400 lines/mm grating were used. A Peltier-cooled CCD detector registered dispersed light with a wavenumber range between 150 and 2500 cm^{-1}. The mapping measurements were carried out using a long working distance ×50 objective due to uneven surface of the samples, the autofocus at each point of the map was used in case of non-flat samples.

All area maps (sampling point spread along X and Y axes) were carried with an exposure time of 4 s with laser power set to 20 mW, and 5 exposures per point using an operating spectral resolution of 4 cm^{-1} of

Table 1
Chemical compositions and physical parameters of the hydroxyapatites used for the fabrication of composites.

Characteristics	Granules	
	HAP	CHAP
Ca/P ratio	1.67	1.69
Fraction size (mm)	0.2–0.6	0.2–0.6
Open porosity (%)	68	66
Surface area (m^2/g)	24	74
Carbonate content (wt.%)[a]	0	5.2

[a] Confirmed by FT-IR and TGA analysis.

Table 2
Chemical compositions and physical parameters of the composite samples used in the study.

Characteristics	Composites	
	HAP/glucan	CHAP/glucan
(HAP or CHAP)/glucan (wt.% ratio)	83:17	83:17
Carbonate content (wt.%)	0	4.3
Compressive strength (MPa)[a]	5.9	6.1
Young's modulus (GPa)[a]	0.78	0.64
Sorption index (%)	121.7	119

[a] Measured for dry composite samples.

Raman shift. For these purposes a 25 μm slit aperture was used and the step between the measurement points was set to 2 μm in both X and Y directions. The cross sections for Raman measurements were prepared by cutting the composites in approximately half of its height and then the samples were air dried. The Raman maps were collected at the edge of the exposed cross section of the surface.

2.3.2.2. Depth profile and statistic. Raman depth profiles (sampling point spread along X and Z axes) were registered using optical slicing capabilities of Raman confocal microscope. Therefore 25 μm pinhole aperture was used. The resulting laser spot size allowed to achieve1-μm spatial resolution and 2-μm depth resolution. The profiles were registered with 1 μm and 0.5 μm steps between the sampling points in X and Z directions respectively. Spectra were acquired with an exposure time of 6 s with laser power set to 20 mW, and 5 exposures per point. The linear depth profiles for statistical analyses of HA distribution in the samples were set to cover around 20 μm (19–30 μm) of the sample surface in the X axis and penetrate the sample to around 10 μm in depth (the Z axis). In the resulting Raman spectral map the size of area adjacent to the sample surface which showed the highest content of the PO_4^{3-} band (980–945 cm^{-1}) characteristic for HA was determined. The area was also used to estimate the thickness of the apatite layer on the sample surface. Five confocal Raman depth profiles of each composite, collected at distinct positions on the sample, were analysed. Obtained values were normalized by length of sampled surface and compered using two-way ANOVA with Tukey's *post hoc* test or Student's unpaired *t*-test (Prism5, GraphPad Software, San Diego). Sampled areas were chosen based on visual inspection of the composite surface. Plain, smooth sections located between HA and CHAP granules, exhibiting spectral feature characteristic for β-1,3-glucan were analysed with focus on small graininess observed on the composite sample surface.

2.4. Weight gain/loss analysis

The sample weight was measured before and after incubation in SBF for 10, 20 and 30 days using balance with an accuracy of 0.1 mg. The percent increases in mass were calculated and compared with mass changes of control scaffolds. The relative standard deviation (RSD) was calculated as repeatability. The percent changes in the mass of materials tested were compared using two-way ANOVA with Bonferroni's *post hoc* test to reveal significant differences between composites and time.

2.5. Ion concentration of the SBF

Reactivity of HAP and CHAP Composites was also discriminated by release/uptake of calcium (Ca^{2+}) and phosphates (PO_4^{3-}). Variations in the concentration of these ions in SBF due to soaking of the scaffolds were verified at defined time points (after 2, 4, 7, 14, 20 and 30 days). The concentrations were measured spectrophotometrically with diagnostic kits: Liquick Cor-Calcium 30 and Liquick Cor-Phosphorus 30 (Cormay, Poland). The statistical significance of changes was evaluated by Student's unpaired *t*-test to reveal differences between both groups for the entire time course.

3. Results

3.1. Surface characterization

3.1.1. SEM images

Morphological changes on the composite surfaces were visible using magnifications higher than 1000×. SEM micrographs of Control sample demonstrated a smooth and homogenous surface of glucan without apatite structures (as shown in Fig. 1A'). After SBF treatment for 30 days, polymeric phases of CHAP and HAP Composites were non-uniformly covered with precipitated calcium phosphates (Fig. 1B' and C'). Careful analysis of multiple images, distinctly revealed that apatite layer on the HAP Composite was thicker than on the CHAP Composite.

3.1.2. Elemental analysis

In order to examine whether the crystallized structures (observed on SEM images) belong to calcium phosphates, EDS analysis were performed. The contents of Ca and P elements were listed in Table 3. It was observed that the chemical composition (Ca, P, C, O and other elements) varied broadly within one scaffold. After soaking in the SBF, the calcium and phosphorus contents increased significantly, indicating deposition of biomimetic apatite. Interestingly, trace amounts of Ca and P were found on untreated samples. The difference between HAP samples after treated in SBF in Ca was 26.9% and 10.6% P. In the CHAP samples the difference was 23% in Ca and 9% in P. Generally the differences between both composites were Ca — 3.9% and P — 1.6% in advantage to the HAP Composite.

3.1.3. Raman spectroscopy and mapping

The spectra of the components of the composites: glucan, HAP, CHAP are presented in Fig. 2. The glucan spectrum presented in Fig. 2A contains bands at 1092, 1366 and 1456 cm^{-1} were assigned to polysaccharides. The typical Raman spectra of the carbonated and non-carbonated hydroxyapatite are presented in Fig. 2B and C. The main band at 961 cm^{-1} is characteristic for the ν_1 PO_4^{3-} vibration. The bands at 1046 and 1069 cm^{-1} are typical for ν_3 PO_4^{3-} vibration. In parallel, carbonate ν_1 mode that is characteristic for substitution type B (PO_4^{3-} substituted by CO_3^{2-}) has also been assigned to the band around 1069 cm^{-1} [41,42]. According to the work of Awonusi et al., decreasing intensity ratio of the bands at 1046 and 1069 cm^{-1}, respectively, signalize increasing carbonate content in hydroxyapatite. Intensity ratio of those bands in CHAP (Fig. 2C) clearly indicates the presence of CO_3^{2-} groups.

The bands marked by the grey frame represent the characteristic fingerprints for each component of the composite. Both carbonated and non-carbonated hydroxyapatites were chosen band typical for phosphate ν_1 PO_4^{3-} at 961 cm^{-1}. Band at 890 cm^{-1} was chosen for localizing polymeric phase (glucan) of composite in the analysed spectra. Both these bands were chosen due to the fact that they gave intensive signals, were easy to detect and did not overlap in both HAP and CHAP types of composites.

Microscopic investigation of the analysed materials revealed existence of rough, granular structures on the surface of the composites soaked in the SBF solution, similar to those observed in the SEM images. Further microspectroscopic analyses showed that they possess spectral features consistent with those observed for hydroxyapatite reference material *e.g.* prominent PO_4^{3-} band at 961 cm^{-1}. Using confocal mode we were able to measure the chemical difference in thin layer on the sample surface. Distribution of PO_4^{3-} band at 961 cm^{-1} showed to coincide with the localization of the structures observed under the microscope as presented in the SEM images Fig. 1. Raman maps collected at the edge of the cross section of the composite showed that the phosphates are spread on the surface in the form of 4–13 μm thin layer (Figs. 3A–D and S1 in Supplementary materials). Further analysis of Raman depth profiles revealed differences in the thickness of the layer between the tested composites (see below). Images excluded possibility that the observed structures possessing apatite like spectral characteristics were part of a bigger hydroxyapatite granule located below the composite surface. Comparison of the maps showed that the apatite like material was present only on the surface of the SBF treated samples. This was truth for both HAP and CHAP Composites suggesting that these materials can accumulate appetite-like material from mineral content of the SBF solution.

The red and green curves in Fig. 3 demonstrate the glucan and phosphate component distribution by normalized band area across the white dotted line marked in the map. In the HAP Control sample Fig. 3A the green line (glucan) is over the red line (phosphates) at the

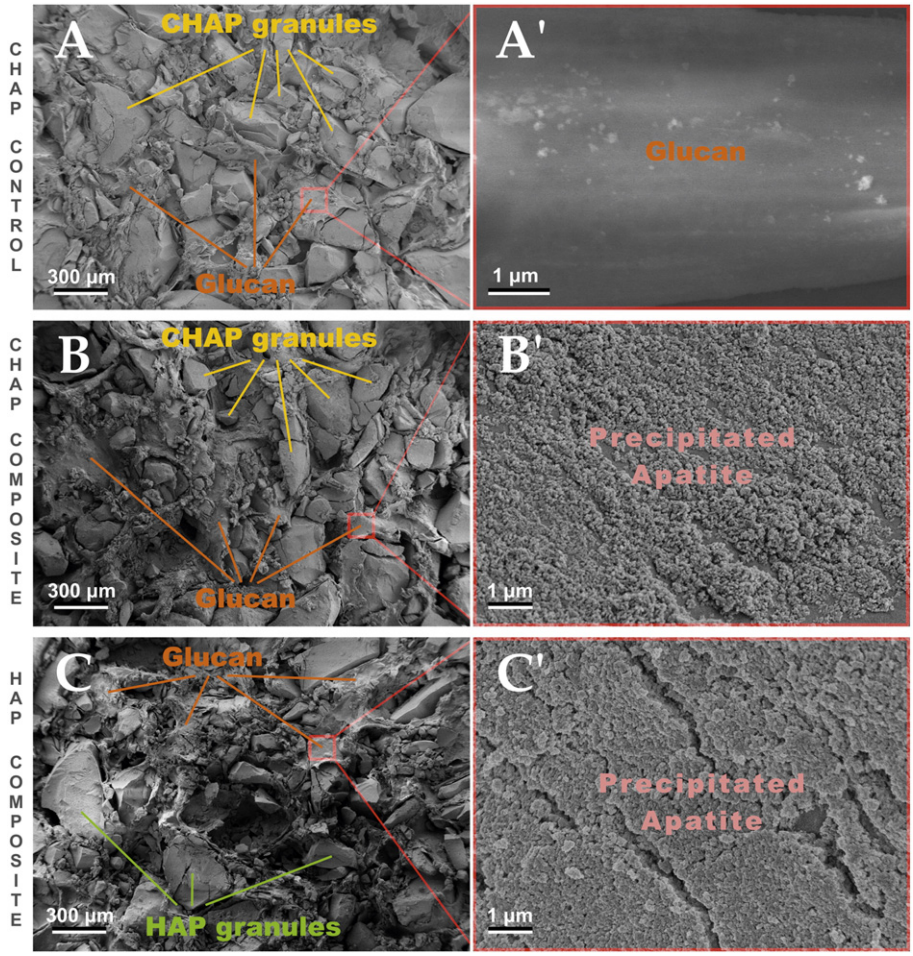

Fig. 1. SEM images of the CHAP Control sample (A) and scaffolds after 30-day SBF treatment: CHAP Composite (B), and HAP Composite (C). A', B' and C' micrographs show magnified fragments of investigated areas (glucan surface).

edge of the sample. Moving toward the inner part of the sample lines change the order. It confirms that in this specific area after the cross section of the sample hydroxyapatite was not present. In Fig. 3B the order of the line is different, which indicate that HA was present in the edge of the sample. The red line profile penetrates deep into the samples together with the distance from the edge. This indicates the presence of surface apatite layer directly into the edge of cross sectioned sample. According to the CHAP Control in Fig. 3C and CHAP Composite Fig. 3D the results are the same as in Fig. 3A and Fig. 3B respectively.

Data derived from confocal Raman depth profiles of analysed samples suggested differences in the abilities of the tested composites to accumulate phosphate ions from surrounding fluids. Data from five confocal Raman depth profiles through the composite surface collected at distinct positions on the sample were analysed. For each, spread of the area showing the highest content of the phosphate PO_4^{3-} band) at 961 cm^{-1} was determined. Obtained data were statistically analysed using two-way ANOVA. Results indicated that HAP Composite binds significantly higher amounts of phosphate ions at the surface than the CHAP Composite (Fig. 4A). Moreover, the thickness of the observed apatite layer at the surface of two tested materials was significantly different (based on the unpaired *t*-test analysis). The average thickness of the

Table 3
Content range of Ca and P elements (in wt.%) on the glucan surface of CHAP and HAP Composites before and after SBF treatment for 30 days.

Sample	SBF	Ca %	P %
CHAP Control	Non-treated	0.5–3	0.2–1
CHAP Composite	Treated (30 days)	1–26	0.3–10
HAP Control	Non-treated	0.5–1.1	0.1–0.4
HAP Composite	Treated (30 days)	1–28	0.4–11

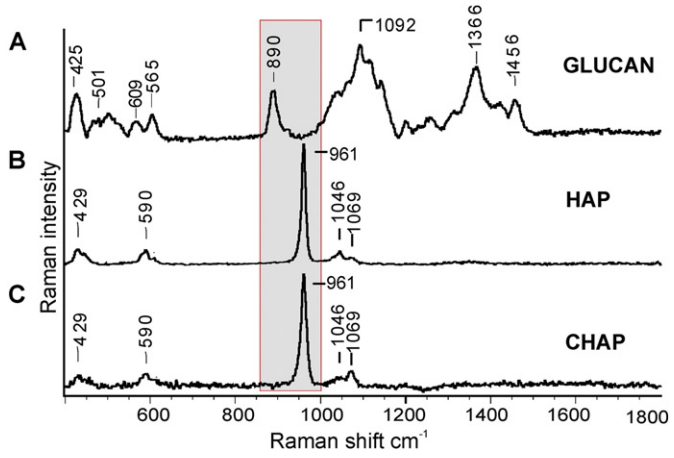

Fig. 2. Raman spectra of A) 1–3-β-D-glucan, B) HAP — non-carbonated hydroxyapatite, C) CHAP — carbonated hydroxyapatite. The grey frame represents fingerprint region for each component.

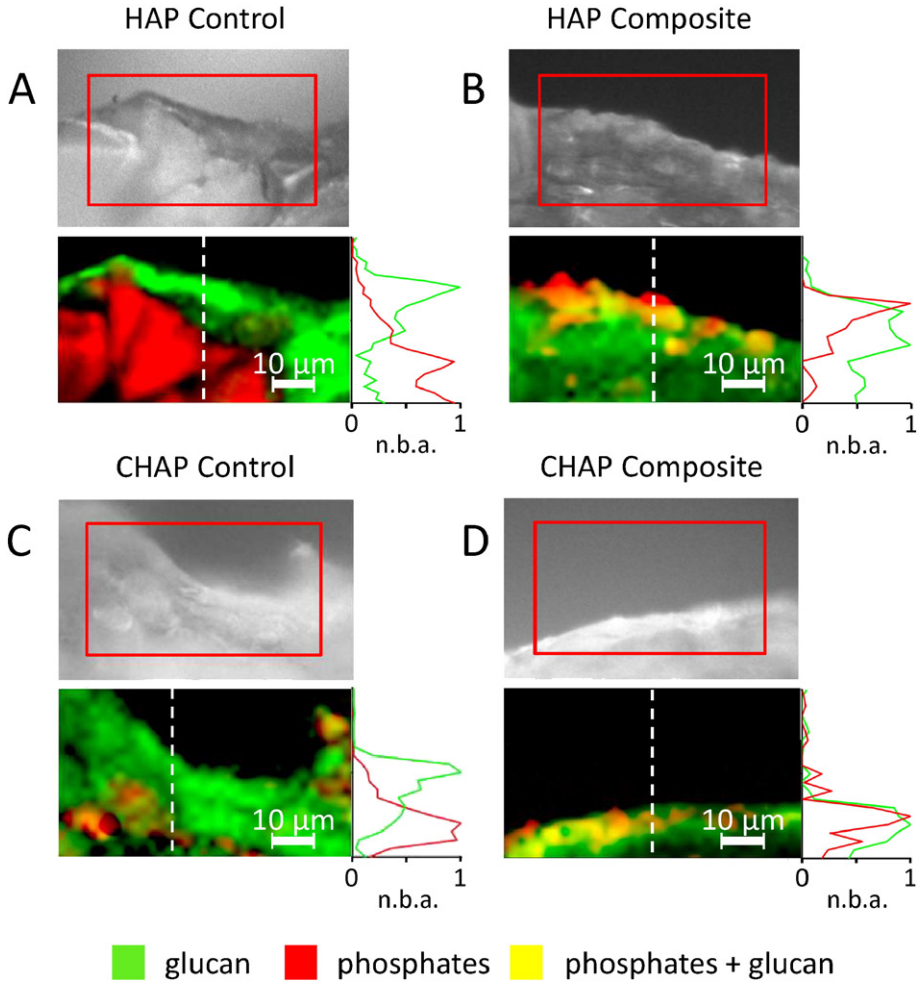

Fig. 3. Raman maps of the edge of the composites after the cross section with the video image and marked area of mapping. The panel A) represents the HAP Control, B) HAP Composite, C) CHAP Control, D) CHAP Composite. The red and green curves show the component distribution by normalized band area (n.b.a.) across the white dotted line marked in the map. The black colour is over the edge of the samples. The green colour represents the spatial distribution of glucan band at 890 cm^{-1}, the red colour — phosphate band at 961 cm^{-1}, the yellow colour — yellow colour the coincide of both bands glucan and phosphates.

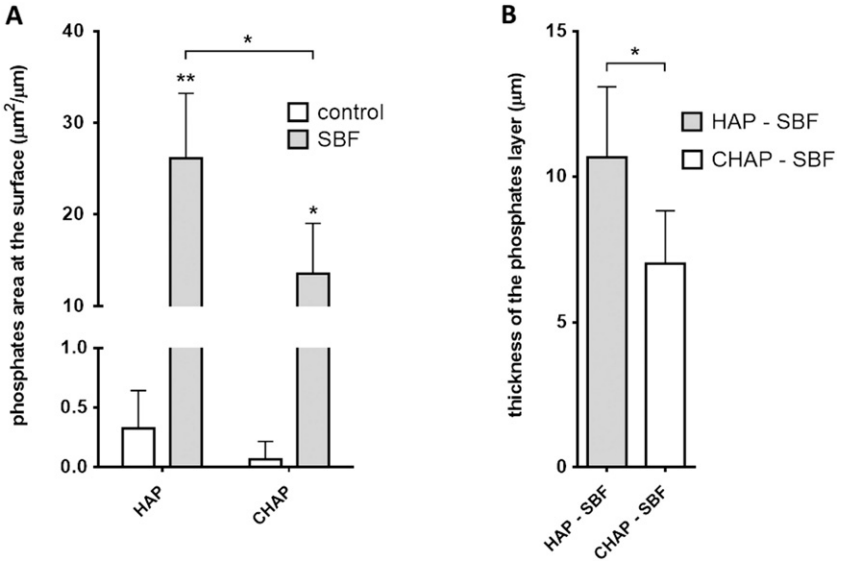

Fig. 4. Analysis of the apatite layer on the surface of the HAP and CHAP Composites based on the Raman depth profiles. Data from five confocal Raman depth profiles for each sample through the surface collected at distinct positions on the sample were analysed. Spread and thickness of the area showing highest content of the PO_4^{3-} band at 961 cm^{-1} across the sampling plane perpendicular to the sample surface were determined. A) Comparison of matrix area occupied by phosphates at the surface of the tested composites. Statistical significance of revealed differences was analysed using two-way ANOVA with Tukey's *post hoc* test. B) Comparison of the thickness of the phosphates layer at the surface of the samples. Statistical significance of reviled differences was analysed using unpaired *t*-test (*$p < 0.01$, **$p < 0.0001$).

layer was estimated to be equal to ~11 μm for HAP and ~7 μm for CHAP Composite (Fig. 4B). Surface apatite width was also illustrated on Fig. S1 in Supplementary materials.

3.2. Mass measurements

The soaking in the SBF solution (renewed every 2–3 days) has influenced weight of samples as observed in Fig. 5. The average weight of CHAP Composite samples gradually increased *i.e.* 2.75% after 10 days and 5.8% after 30 days. The weight gain of HAP Composite samples tended to be higher ($p < 0.0001$) with an average of 4.5% after 10 days and 7.73% after 30 days. These changes were in contrast to weight of Control samples (incubated in water for 30 days) which achieved 1.63% and 0.68% weight loss for CHAP and HAP Composites, respectively.

3.3. Ion changes in SBF

Ion reactivity of biomaterials was evaluated by measurement of the element concentrations in the SBF solution. Both of the examined materials showed substantial changes in the calcium concentration of the SBF (Fig. 6A). It was found that 2-day incubation of CHAP Composite scaffolds decreased significantly the Ca^{2+} concentration from 2.5 mM to 1.37 mM. HAP Composite also caused decrease in calcium concentration to 1.08 mM. During the next days of experiment Ca^{2+} concentrations decreased to similar level and after 30 days amounted 1.35 mM and 1.27 mM for CHAP and HAP Composites, respectively. Furthermore, the results showed significantly higher absorption of calcium ions by HAP Composite (unpaired *t*-test; $p = 0.005$), mainly noticeable between 2 and 7 days of experiment. Fig. 6B showed the decrease in phosphate concentration of SBF and the statistical analysis revealed non-significant difference between both materials ($p \geq 0.05$). Initially, *i.e.* after 2 days, concentration of these ions decreased by approx. 80% from 0.9 mM below 0.2 mM. In the next days of experiment the measurements indicated that the drop in phosphate concentration was gradually smaller.

4. Discussion

Successful regeneration of bone tissue depends primarily on properties of implanted materials such as bioactivity and biocompatibility. These features may be predicted with *in vitro* tests prior to doing time and money consuming *in vivo* studies and can significantly reduce the number of experimental animals [28]. Two most common bioactivity tests include the apatite-formation ability of biomaterials in the SBF and *in vitro* bone cell response to biomaterials. Bioactivity tests in SBF may be conducted under static or dynamic conditions, however, immersion in dynamic SBF can better simulate conditions of bone-like apatite formation in human body than that in static SBF, which was used in most *in vitro* research [43]. There were several studies, such as Szubert et al., [44] and ours (Unpublished results) which showed that regular replacement of SBF solution increased apatite layer formation.

Hydroxyapatite has been frequently used for bone and dental implant fabrication. Since its development, there has been a lot of work investigating the effect of its formulation and structure on bone regeneration process. However, many of the research lack direct comparison of non-substituted ("pure") HAP with carbonate-substituted form which is recently studied, due to its higher compositional similarity to mineral of bone and dentine. As mentioned earlier, the rate of apatite formation determines the bone bonding ability of bioactive materials, thus ion reactivity of both hydroxyapatites must be considered. *In vitro* bone cell response to HAP and CHAP was compared earlier and the results of MTT and NRU tests showed some cytotoxic effect on hFOB and HSF cells, greater for HAP, due to its higher uptake of calcium ions from a cell culture medium [45]. In the present study apatite-forming ability of both hydroxyapatites was examined with the use of polymer containing composites under semi-dynamic SBF conditions. The physicochemical data of the HAP and CHAP granules were described in our previous articles and 2 european patents [35,38,39,46].

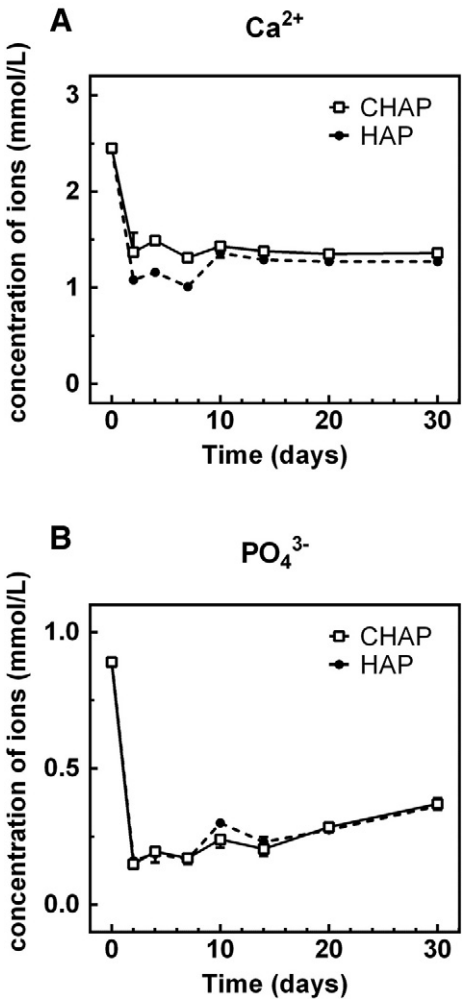

Fig. 6. Variations in the calcium Ca^{2+} (A) and phosphates PO_4^{3-} (B) concentration of SBF due to soaking of the scaffolds for 30 days.

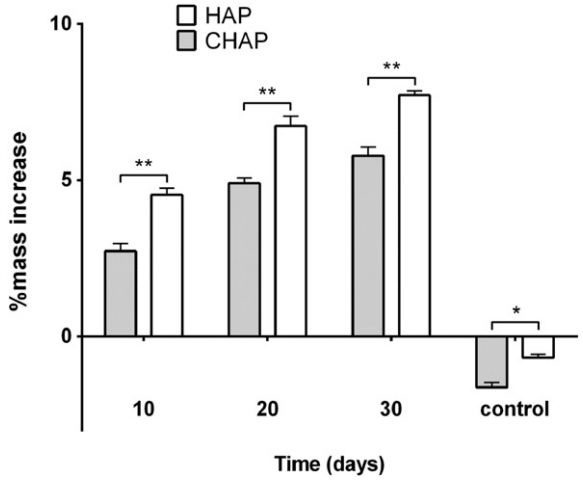

Fig. 5. The weight change of scaffolds after SBF treatment for 10, 20 and 30 days (expressed as wt.%). Column C represents Control samples incubated in water for 30 days. Statistical significance of revealed differences was analysed using two-way ANOVA with Bonferroni's *post hoc* test (*$p < 0.01$, **$p < 0.0001$).

The data presented here, documented by SEM–EDS, Raman mapping, scaffold mass measurements and ion changes in SBF, indicate higher bioactive properties of non-substituted hydroxyapatite. HAP exhibited superior ionic reactivity and apatite-formation potential.

From the SEM images shown in Fig. 1A, B and C, it can be observed that scaffold microarchitecture has a high porosity and opened pore structure. It may be noted that the matrix is composed of β-1,3-glucan and the surface of the matrix is coated with apatite in the form of fine crystals (Fig. 1B' and C'). Both SBF-treated composites showed the presence of crystallites, mostly in the form of thin apatite layer. The wide range of apatite particles on the scaffold surface can give more contacting areas for bone cell deposition that is a benefit for the biomineralization. From the work of Kawashita et al. [37], it is known that pure β-1,3-glucan is an inert material in SBF and it does not induce apatite formation.

All the EDX data collected (Table 3) indicated significant increase of Ca and P elements in comparison with Control samples. Collation of Ca and P contents between SBF-treated samples unveiled the wider range of these elements on HAP Composite glucan surface: 3.9% and 1.6% for Ca and P, respectively. Presented data are in line with our previous work, performed for CHAP Composite under static SBF conditions, where we reported differences in chemical composition within one scaffold and non-uniform arrangement of emerging apatite [47]. This study in semi-dynamic SBF conditions confirmed our previous observation that apatite crystals arranged on the glucan surface heterogeneously.

SEM/EDS studies of SBF non-treated composites brought another interesting observation. On the superficial area of organic phase of both composites, some calcium phosphates were detected, most probably due to scaffold preparation process, which left some small granule wreckages that we called “apatite dust”. However, as shown in Table 3, it did not distort the total result, because the content of Ca and P elements on SBF treated samples was significantly (at least 10 times) greater.

The presence of new apatite layer was confirmed as well by Raman maps collected at the edge of the cross section of the composites (Fig. 3) and analysis of polymer surface occupied by phosphates (Fig. 4A). High content of the apatite like material at the surface of the SBF-treated scaffolds, indicated by abundance of PO_4^{3-} band at glucan area, supported previous conclusions. The thickness of new hydroxyapatite layer was measured using confocal Raman depth profiles and confirmed SEM result (Figs. 4B and S1 in Supplementary materials). The thickness of apatite layer was between 4 and 13 μm, and was comparable to that obtained by Yu et al. [48], for 40 vol.% HA/PEEK composite immersed in SBF for 14 and 28 days. Moreover, the resulting maps showed that the apatite layer in a high degree overlaps with the underlying glucan component. This suggested that the newly deposited apatite can also infiltrate glucan. However, it has to be noted that the resolution of the depth profiles is limited due to optical properties of instrument (2 μm in the Z axis) and the nature of the analysis. Even that measurements were done in confocal mode some of the signal from the upper parts may contribute to the signal registered for the lower levels of the sampled depth profile. This may lead to tailing of the strong PO_4^{3-} band toward deeper fractions of the sampled area and therefore, result in some overestimation in the thickness of the surface apatite layer. Thus caution is recommended when interpreting the results.

The use of different Raman spectroscopy approaches combined with SEM images allowed to look at the sample surface from a distance of different perspectives: micro — Raman mapping (70 × 50 μm map area), and macro/micro — SEM images. The use of confocal depth profiles as an noninvasive technique made it possible to show the cross section into the specimen without disturbing its structure. The complementarity of SEM and different Raman approaches *e.g.* spatial distribution and depth profiles were presented.

The weight measurements demonstrated mass increase for SBF-treated samples (Fig. 5) and showed significantly greater weight gain for HAP Composite ($p < 0.0001$). The degradation loss was higher among CHAP-containing samples in accordance with [49,50]. The estimated newly formed apatite (precipitation rate) was about 7.43% and 8.41% for CHAP and HAP Composites, respectively. Hence, the difference of the newly formed apatite amounted to approximately 0.98%. The weight measurements correspond to the decreased concentration of calcium and phosphorus ions in SBF caused by both types of composite (Fig. 6). During 4 weeks, HAP Composite exhibited significantly higher uptake of calcium ions from SBF than CHAP Composite, most distinctly during first 7 days.

Overall, apatite-forming abilities were comparable in both groups indicating that the non-substituted HAP influenced insignificantly higher bioactive properties of glucan-containing composite. However, some studies report that carbonate substitution within hydroxyapatite increases the solubility and decreases the crystallinity of ceramics, thus CHAP was expected to exhibit higher apatite-forming ability than HAP [3,4]. Our results do not confirm this statement. It may be explained that both composites require various chemical element balances (mainly dealing with calcium and phosphates) of the SBF solution, needed for nucleation — initial step of precipitation process. Another theory is that, increased solubility of carbonate-substituted HAP do not indicate greater apatite formation, due to the shift of elemental balance into a lower apatite crystallization. It is also possible that interactions between organic part of composite — glucan and inorganic phase — ceramic hydroxyapatite affect the crystallization process of new hydroxyapatite layer on the composite surface and interfere ion exchange/balance process. In the literature, we found several other factors that may be taken into consideration. According to McLeod et al., apatite deposition *via* SBF may be inconsistent with wide variations across a substrate due to the surface tension of the fluid *versus* the substrate [51]. Barrere et al., [52] reported that increased concentration of HCO_3^- in SBF inhibits apatite crystal growth, which corresponds to our results of higher CHAP degradation than HAP. Moreover, Müller and Müller [53] claimed that the HCO_3^- content in SBF influences the size of apatite crystallites. Briefly, the higher HCO_3^- content, the lower crystallites formed. Presumably, this mechanism also may affect precipitation rate.

5. Conclusions

Bone tissue engineering dispose with two types of hydroxyapatite for the construction of scaffolds: and biomimetic, carbonate-substituted hydroxyapatite. Detailed comparison of their properties is under continuous investigation. In our study we attempted to assess their bioactivity in acknowledged SBF solution. The results did not prove higher apatite-forming ability of carbonate hydroxyapatite in comparison to non-substituted HAP. Meanwhile, we report the noticeable differences in calcium uptake and the thickness of the observed newly-precipitated apatite structures. The results confirmed higher degradation rate of carbonate hydroxyapatite. Our studies could provide useful insights for designing bioapatites with optimized performance for bone tissue engineering.

Supplementary data to this article can be found online at http://dx.doi.org/10.1016/j.msec.2016.01.056.

Acknowledgements

The authors would like to acknowledge that the financial assistance for this research was provided by the Medical University in Lublin (DS2) and by the Medical University Student Grant Program awarded to Leszek Borkowski (MMsd 3). The authors would especially like to express their gratitude to Prof. Krzysztof Jóźwiak and Prof. Dariusz Matosiuk for the use of their spectroscopic equipment. Finally, ASB and PD would like to acknowledge the Foundation for Polish Science (TEAM Programme 2009-4/5).

References

[1] L.L. Hench, Bioceramics: from concept to clinic, J. Am. Ceram. Soc. 74 (7) (1991) 1487–1510.
[2] A. Bigi, G. Cojazzi, S. Panzavolta, A. Ripamonti, N. Roveri, M. Romanello, K. Noris Suarez, L. Moro, Chemical and structural characterization of the mineral phase from cortical and trabecular bone, J. Inorg. Biochem. 68 (1997) 45–51.
[3] Y.P. Guo, Y.B. Yao, Y.J. Guo, C.Q. Ning, Hydrothermal fabrication of mesoporous carbonated hydroxyapatite microspheres for a drug delivery system, Microporous Mesoporous Mater. 155 (2012) 245–251.
[4] M.H. Fathi, A. Hanifi, V. Mortazavi, Preparation and bioactivity evaluation of bone-like hydroxyapatite nanopowder, J. Mater. Process. Technol. 202 (2008) 536–542.
[5] F. Barrere, P. Layrolle, C.A. van Blitterswijk, K. de Groot, Biomimetic calcium phosphate coatings on Ti6A14V: a crystal growth study of octacalcium phosphate and inhibition by Mg 2+ and HCO 3−, Bone 25 (2) (1999) 107S–111S.
[6] F. Barrere, C.M. Van der Valk, G. Meijer, R.A.J. Dalmeijer, K. De Groot, P. Layrolle, Osteointegration of biomimetic apatite coating applied onto dense and porous metal implants in femurs of goats, J. Biomed. Mater. Res. B Appl. Biomater. 67 (1) (2003) 655–665.
[7] L. Jonášová, F.A. Müller, A. Helebrant, J. Strnad, P. Greil, Biomimetic apatite formation on chemically treated titanium, Biomaterials 25 (7) (2004) 1187–1194.
[8] W.H. Song, Y.K. Jun, Y. Han, S.H. Hong, Biomimetic apatite coatings on micro-arc oxidized titania, Biomaterials 25 (17) (2004) 3341–3349.
[9] L. Müller, E. Conforto, D. Caillard, Müller F. A., Biomimetic apatite coatings—carbonate substitution and preferred growth orientation, Biomol. Eng. 24 (5) (2007) 462–466.
[10] C. Du, F.Z. Cui, W. Zhang, Q.L. Feng, X.D. Zhu, K. de Groot, Formation of calcium phosphate/collagen composites through mineralization of collagen matrix, J. Biomed. Mater. Res. 50 (2000) 518–527.
[11] C. Du, G.J. Meijer, C. Van de Valk, R.E. Haan, J.M. Bezemer, S.C. Hesseling, F.Z. Cui, K. de Groot, P. Layrolle, Bone growth in biomimetic apatite coated porous polyactive® 1000PEGT70PBT30 implants, Biomaterials 23 (23) (2002) 4649–4656.
[12] M. Lee, W. Li, R.K. Siu, J. Whang, X. Zhang, C. Soo, K. Ting, B.M. Wu, Biomimetic apatite-coated alginate/chitosan microparticles as osteogenic protein carriers, Biomaterials 30 (30) (2009) 6094–6101.
[13] H. Nagai, M. Kobayashi-Fujioka, K. Fujisawa, G. Ohe, N. Takamaru, K. Hara, Y. Miyamoto, Effects of low crystalline carbonate apatite on proliferation and osteoblastic differentiation of human bone marrow cells, J. Mater. Sci. Mater. Med. 26 (2) (2015) 1–8.
[14] E. Landi, G. Celotti, G. Logroscino, A. Tampieri, Carbonated hydroxyapatite as bone substitute, J. Eur. Ceram. Soc. 23 (2003) 2931–2937.
[15] R. Zagury, N.D. Harari, M.B. Conz, Soares G. de Almeda, G.M. Vidigal, Histomorphometric analyses of bone interface with titanium-aluminium-vanadium and hydroxyapatite-coated implants by biomimetic process, Implant. Dent. 16 (2007) 290–296.
[16] B. Li, X. Liao, L. Zheng, H. He, H. Mang, H. Fan, X. Zhang, Preparation and cellular response of porous A-type carbonated hydroxyapatite nanoceramics, Mater. Sci. Eng. C Mater. Biol. Appl. 32 (2012) 929–936.
[17] S. Kannan, S.I. Vieira, S.M. Olhero, P.C.M. Torres, S. Pina, O.A.B. da Cruz e Silva, J.M.F. Ferreira, Synthesis, mechanical and biological characterization of ionic doped carbonated hydroxyapatite/β-tricalcium phosphate mixtures, Acta Biomater. 7 (2011) 1835–1843.
[18] R. Detsch, D. Hagmeyer, M. Neumann, S. Schaefer, A. Vortkamp, M. Wuelling, The resorption of nanocrystalline calcium phosphates by osteoclast-like cells, Acta Biomater. 6 (2010) 3223–3233.
[19] A. Yoshida, T. Miyazaki, M. Ashizuka, E. Ishida, Bioactivity and mechanical properties of cellulose/carbonate hydroxyapatite composites prepared in situ through mechanochemical reaction, J. Biomater. Appl. 21 (2) (2006) 179–194.
[20] Z. Hong, P. Zhang, A. Liu, L. Chen, X. Chen, X. Jing, Composites of poly (lactide-co-glycolide) and the surface modified carbonated hydroxyapatite nanoparticles, J. Biomed. Mater. Res. A 81 (3) (2007) 515–522.
[21] W. Linhart, F. Peters, W. Lehmann, K. Schwarz, A.F. Schilling, M. Amling, J.M. Rueger, M. Epple, Biologically and chemically optimized composites of carbonated apatite and polyglycolide as bone substitution materials, J. Biomed. Mater. Res. 54 (2) (2001) 162–171.
[22] L. Zheng, F. Yang, H. Shen, X. Hu, Ch. Mochizuki, M. Sato, S. Wang, Y. Zhang, The effect of composition of calcium phosphate composite scaffolds on the formation of tooth tissue from human dental pulp stem cells, Biomaterials 32 (2011) 7053–7059.
[23] G.L. Yang, F.M. He, J.A. Hu, X.X. Wang, S.F. Zhao, Effects of biomimetically and electrochemically deposited nano-hydroxyapatite coatings on osseointegration of porous titanium implants, Oral Maxilofac. Impants 107 (2009) 782–789.
[24] H. Suh, C. Lee, Biodegradable ceramic—collagen composite implanted in rabbit tibiae, ASAIO J. 41 (3) (1995) M652–M656.
[25] Y. Shikinami, Y. Matsusue, T. Nakamura, The complete process of bioresorption and bone replacement using devices made of forged composites of raw hydroxyapatite particles/poly l-lactide (Fu-HA/PLLA), Biomaterials 26 (27) (2005) 5542–5551.
[26] S. Hasegawa, J. Tamura, M. Neo, K. Goto, Y. Shikinami, M. Saito, M. Kita, T. Nakamura, In vivo evaluation of a porous hydroxyapatite/poly-DL-lactide composite for use as a bone substitute, J. Biomed. Mater. Res. A 75 (3) (2005) 567–579.
[27] Q.L. Li, M.Y. Wu, L.L. Tang, J. Zhou, Y. Jiang, B.W. Darvell, Bioactivity of a Novel Nano—composite of hydroxyapatite and chitosan-phosphorylated chitosan polyelectrolyte complex, J. Bioact. Compat. Polym. 23 (6) (2008) 520–531.
[28] T. Kokubo, H. Takadama, How useful is SBF in predicting in vivo bone bioactivity? Biomaterials 27 (15) (2006) 2907–2915.
[29] T. Kokubo, H. Kushitani, S. Sakka, T. Kitsugi, T. Yamamuro, Solutions able to reproduce in vivo surface-structure changes in bioactive glass — ceramic A-W3, J. Biomed. Mater. Res. 24 (1990) 721–734.
[30] Y. Abe, T. Kokubo, T. Yamamuro, Apatite coating on ceramics, metals and polymers utilizing a biological process, J. Mater. Sci. Mater. Med. 1 (4) (1990) 233–238.
[31] Y.F. Chou, W. Huang, J.C. Dunn, T.A. Miller, B.M. Wu, The effect of biomimetic apatite structure on osteoblast viability, proliferation, and gene expression, Biomaterials 26 (3) (2005) 285–295.
[32] B. Fang, Y.Z. Wan, T.T. Tang, C. Gao, K.R. Dai, Proliferation and osteoblastic differentiation of human bone marrow stromal cells on hydroxyapatite/bacterial cellulose nanocomposite scaffolds, Tissue Eng. A 15 (5) (2009) 1091–1098.
[33] A. Przekora, J. Czechowska, D. Pijocha, A. Ślósarczyk, G. Ginalska, Do novel cement-type biomaterials reveal ion reactivity that affects cell viability in vitro? Cent. Eur. J. Biol. 9 (3) (2014) 277–289.
[34] C. Wu, Y. Xiao, Evaluation of the in vitro bioactivity of bioceramics, Bone Tissue Regen. Insights 2 (2009) 25–29.
[35] A. Belcarz, G. Ginalska, T. Pycka, A. Zima, A. Ślósarczyk, I. Polkowska, Z. Paszkiewicz, W. Piekarczyk, Application of β-1, 3-glucan in production of ceramics-based elastic composite for bone repair, Cent. Eur. J. Biol. 8 (6) (2013) 534–548.
[36] L. Borkowski, M. Pawłowska, R.P. Radzki, M. Bieńko, I. Polkowska, A. Belcarz, M. Karpiński, T. Słowik, L. Matuszewski, A. Ślósarczyk, G. Ginalska, Effect of a carbonated HAP/β-glucan composite bone substitute on healing of drilled bone voids in the proximal tibial metaphysis of rabbits, Mater. Sci. Eng. C 53 (2015) 60–67.
[37] M. Kawashita, M. Nakao, M. Minoda, H.M. Kim, T. Beppu, T. Miyamoto, T. Kokubo, T. Nakamura, Apatite-forming ability of carboxyl group-containing polymer gels in a simulated body fluid, Biomaterials 24 (14) (2003) 2477–2484.
[38] Belcarz A, Ginalska G, Ślósarczyk A, Paszkiewicz Z. (2010). Bioactive composite and process for the production of the bioactive composite. European Patent EP107266397
[39] Paszkiewicz Z, Ślósarczyk A, Zima A. (2011). Method for fabrication of synthetic bioceramic implant material based on carbonate hydroxyapatites. European Patent EP233853140
[40] Ślósarczyk A, Paszkiewicz Z, Zima A. (2014). Method for fabrication of highly porous, calcium phosphate bioactive implant material. European Patent EP2229961
[41] G. Penel, G. Leroy, C. Rey, E. Bres, MicroRaman spectral study of the PO4 and CO3 vibrations modes in synthetic and biological appatites, Calcif. Tissue Int. 63 (1998) 475–481.
[42] A. Awonusi, M.D. Morris, M.M. Tecklenburg, Carbonate assignment and calibration in the Raman spectrum of apatite, Calcif. Tissue Int. 81 (1) (2007) 46–52.
[43] Y.R. Duan, Z.R. Zhang, C.Y. Wang, J.Y. Chen, X.D. Zhang, Dynamic study of calcium phosphate formation on porous HA/TCP ceramics, J. Mater. Sci. Mater. Med. 16 (9) (2005) 795–801.
[44] M. Szubert, K. Adamska, M. Szybowicz, T. Jesionowski, T. Buchwald, A. Voelkel, The increase of apatite layer formation by the poly (3-hydroxybutyrate) surface modification of hydroxyapatite and β-tricalcium phosphate, Mater. Sci. Eng. C 34 (2014) 236–244.
[45] A. Przekora, D. Kołodyńska, G. Ginalska, A. Ślósarczyk, The effect of biomaterials ion reactivity on cell viability in vitro, Eng. Biomater. 15 (114) (2012) 59–65.
[46] J. Kolmas, A. Jaklewicz, A. Zima, M. Bućko, Z. Paszkiewicz, J. Lis, A. Ślósarczyk, W. Kolodziejski, Incorporation of carbonate and magnesium ions into synthetic hydroxyapatite: the effect on physicochemical properties, J. Mol. Struct. 987 (1) (2011) 40–50.
[47] L. Borkowski, G. Ginalska, A. Ślósarczyk, Z. Paszkiewicz, Apatite formation on a flexible bone substitute, Eng. Biomater. 14 (106/108) (2011) 105–109.
[48] S. Yu, K.P. Hariram, R. Kumar, P. Cheang, K.K. Aik, In vitro apatite formation and its growth kinetics on hydroxyapatite/polyetheretherketone biocomposites, Biomaterials 26 (15) (2005) 2343–2352.
[49] D.G.A. Nelson, The influence of carbonate on the atomic structure and reactivity of hydroxyapatite, J. Dent. Res. 60 (3) (1981) 1621–1629.
[50] M.T. Fulmer, I.C. Ison, C.R. Hankermayer, B.R. Constantz, J. Ross, Measurements of the solubilities and dissolution rates of several hydroxyapatites, Biomaterials 23 (3) (2002) 751–755.
[51] K. McLeod, S. Kumar, N.K. Dutta, R.S.C. Smart, N.H. Voelcker, G.I. Anderson, X-ray photoelectron spectroscopy study of the growth kinetics of biomimetically grown hydroxyapatite thin-film coatings, Appl. Surf. Sci. 256 (23) (2010) 7178–7185.
[52] F. Barrere, C.A. Van Blitterswijk, K. De Groot, P. Layrolle, Influence of ionic strength and carbonate on the Ca-P coating formation from SB × 5 solution, Biomaterials 23 (9) (2002) 1921–1930.
[53] L. Müller, F.A. Müller, Preparation of SBF with different content and its influence on the composition of biomimetic apatites, Acta Biomater. 2 (2) (2006) 181–189.